Limnol. Oceanogr., 55(3), 2010, 1231–1247

doi:10.4319/lo.2010.55.3.1231

Oscillatory porewater bioadvection in marine sediments induced by hydraulic activities of *Arenicola marina*

N. Volkenborn,[a,b,*] L. Polerecky,[c] D. S. Wethey,[a,b] and S. A. Woodin,[a,b]

[a] Department of Biological Sciences, University of South Carolina, Columbia, South Carolina
[b] Alfred Wegener Institute for Polar and Marine Research in the Helmholtz Association, Wadden Sea Station Sylt, List, Germany
[c] Max-Planck-Institute for Marine Microbiology, Bremen, Germany

Abstract

We employed real-time pressure recording and high temporal resolution two-dimensional oxygen imaging to characterize the porewater bioadvection related to hydraulic activities of *Arenicola marina*, a widespread representative of benthic macrofauna. Behavior-specific positive and negative pressure oscillations and hydraulic pulses resulted in bidirectional porewater flow and highly dynamic redox oscillations on the scale of minutes. Pumping of water by the worm into its blind-ending burrow pressurized the sediment and caused sediment oxygenation at depth and the exit of anoxic porewater into the overlying water. The sediment volume that was affected by bioadvective transport of oxygen and the porewater flow patterns varied strongly among sediment types. In low-permeability sediments, localized plumes of anoxic porewater ascended from the sediment, presumably through sedimentary cracks, while porewater flowed evenly through highly permeable sediments. Hydraulic behaviors that moved water out through the open tail shaft caused a reduction of porewater pressures below the hydrostatic baseline which resulted in the collapse of plumes and enhanced oxygen penetration into the surficial sediments. Porewater bioadvection and the related perfusing and oscillatory phenomena will affect a variety of biogeochemical and ecological processes, including organic matter mineralization, benthic recruitment, and prey localization. We suggest that bidirectional porewater bioadvection and the associated transient geochemical conditions are prevalent features of biogenically active sediments.

Oceans cover ~ 70% of the Earth, and most of the seafloor is sedimentary (Snelgrove et al. 1997; Teal et al. 2008). Thus, marine sediments constitute the most extensive benthic ecosystem on our planet in areal coverage. Since the Cambrian explosion more than 500 million years ago, the ocean seafloor has evolved from a mostly layered system, dominated by microbial mats, to a bulldozed environment populated by diverse bottom-dwelling assemblages (Thayer 1979; Cadée 2001; Meysman et al. 2006*a*). Infaunal activities strongly affect benthopelagic exchange processes and biogeochemical cycling (Aller 2001; Lohrer et al. 2004; Kogure and Wada 2005). On average, the upper 5–10 cm of the seafloor is biologically mixed (Boudreau 1998), implying that bioturbation by benthic organisms plays an important role in the global cycling of material. This upper sediment layer is a diagenetic hotspot where high densities of microbes use deposited organic material for their metabolism, employing a variety of electron acceptors (e.g., oxygen, nitrate, oxidized iron, sulfate) (Canfield et al. 1993; Thamdrup and Canfield 2000). Importantly, both the availability and transport of the organic material and the electron acceptors are strongly affected by the activities of the bottom-dwelling organisms, particularly the large infauna (Kristensen 1988; Ziebis et al. 1996; Glud 2008).

In very low permeability sediments, infaunal activities displace sediment particles and move water within the burrow lumen. In such sediments, exchange of burrow water with porewater is limited and solute transport is governed by diffusion (except during burrowing). These conditions are implemented in traditional models of bioirrigated sediments (Aller 1980). In more permeable sediments, the assumption of diffusion as the predominant mode of transport is still valid if the burrow lining is robust and complete and two or more surface openings are present. Note that we are ignoring the contribution of surface topography and physical advection (Huettel et al. 1996). In some cases the burrow lining may actually inhibit diffusion (Aller and Yingst 1978; Aller 1983; Riisgård and Larsen 2005). However, some benthic animals have blind-ending burrows (e.g., arenicolid polychaetes, Kristensen 2001), excurrent siphons below the sediment surface (e.g., tellinid bivalves, Reise 1983), or incomplete or very porous burrow linings (e.g., some nereid polychaetes, Wethey and Woodin 2005; some thalassinid crustaceans, the authors with T. Dewitt unpubl. data) and pump water into subsurface sediments. In addition to the diffusive transport that occurs between burrow lumen and surrounding sediment, such bottom-dwelling organisms induce the movement of interstitial water through the sediment surrounding the burrow, a phenomenon hereafter called porewater bioadvection. With porewater bioadvection both water and solutes are exchanged and the transport rates are typically much faster and affect greater sediment volumes than in diffusive systems. This concept is implemented in more recently developed models of bioirrigation in permeable sediments (Timmerman et al. 2002; Meysman et al. 2005) as well as in mechanical devices that are used to mimic infaunal hydraulic activities (Na et al. 2008). However, these models and mimics assume that infauna act as continuous and unidirectional mechanical pumps, which oversimplifies the reality (Wells 1963; Krüger 1964;

* Corresponding author: nils@biol.sc.edu

Timmerman et al. 2006). They ignore several common behaviors with potentially important consequences, which are the focus of this paper.

Porewater bioadvection is a function of infaunal activity, which varies greatly with time in both rate and direction (Krüger 1964). If the organism ceases to be active or reverses the direction of its pumping, advection correspondingly stops or reverses direction. Such alterations in rate and direction in bioadvective porewater transport can lead to oscillations in microenvironmental parameters on the scale of minutes to hours, with important consequences for sediment biogeochemistry (Timmermann et al. 2006). Redox oscillations, for example, are a likely consequence and are known to increase organic matter degradation rates, both in diffusive and bioadvective systems (Aller 1994; Sun et al. 2002). Other examples of how perturbations influence the activity of microbial communities, although not necessarily in sediments, include a complex nitrifying and denitrifying microbial community, whose perturbation with oxygen or NO_2^- leads within minutes to the release of NO and N_2O, an important signaling molecule and a potent greenhouse gas, respectively (Schreiber et al. 2009), or denitrifying bacteria ingested by aquatic invertebrates, which release significant amounts of N_2O as a consequence of fluctuations between anoxic and oxic conditions while the bacteria pass through the animal gut, a process that is not long enough to allow complete denitrification (Stief et al. 2009). Thus, by inducing oscillatory perturbations to the microenvironment on short temporal scales, and by affecting large sediment volumes, porewater bioadvection is expected to have significant effects on microbial activity and biogeochemical conversion processes in sediments.

To quantify these oscillations in the sedimentary microenvironment and assess their effect on sediment biogeochemistry, they must be resolved by experimental approaches on the relevant spatial and temporal scales. The development of field deployable pressure sensors allows detection of activities of unrestrained infauna and observation of the dynamics of their biohydraulic activities on timescales of seconds (Wethey and Woodin 2005). Pressure records for *Arenicola marina* indicate that the direction and magnitude of porewater bioadvective fluxes change on the scale of minutes and can be detected up to 50 cm away from the animal (Wethey et al. 2008). However, the porewater pressure sensor technology alone does not allow quantitative assessment of biogeochemical dynamics associated with macrofaunal activity. In principle, microelectrodes could be used for this purpose. They yield sufficient spatial and temporal resolutions, but the need for a large number of sensing points to satisfactorily describe the spatiotemporal dynamics in bioirrigated sediments makes this approach very difficult. A possible alternative is offered by the planar optode based imaging technology, introduced in the field of sediment biogeochemistry by Glud et al. (1996). By allowing monitoring of sedimentary oxygen dynamics in two dimensions and with a temporal resolution of a few seconds, this technique is highly suited for bioirrigation studies (Polerecky et al. 2006). In a case study, we combined this imaging technique with the porewater pressure sensors and visible-light imagery to assess, both qualitatively and quantitatively, how the activities of the widespread abundant lugworm *A. marina* affect the spatial and temporal patterns of porewater flow and redox oscillations in various sediment types.

Methods

Experimental setup—A. marina lives in up to 40-cm deep, J-shaped blind-ending burrows, feeding on surface material subducted to depth, and defecating on the sediment surface (Wells 1963; Riisgård and Banta 1998) (*see* Web Appendix, Video 1; www.aslo.org/lo/toc/vol_55/issue_3/1231a.html). To allow for the establishment of similar conditions during the experiment, individual lugworms were kept in sandwich aquaria filled to a depth of 20 cm with natural sediment and supplied with oxygenated seawater recirculating over the surface. Aquaria consisted of two acrylic panels (40 × 30 cm) tightly screwed against a Tygon© sidewall, resulting in an aquarium that was 1.2-cm wide and contained 0.72 liters of sediment and 0.18 liters of overlying water. Sediments were collected from six intertidal areas near the island of Sylt, Germany (55°02′N, 8°24′E), with different sediment characteristics, ranging from coarse sand (grain size median 350 μm, silt content ~ 0.1%) to fine sand (grain size median 200 μm, silt content ~ 1%). Three different layers were sampled separately: oxidized surface sediment (brownish, top 1–2 cm), reduced subsurface sediment rich in iron sulfide precipitates (black, ~ 15 cm), and FeS_2 rich subsurface sediment (gray, ~ 3 cm). Sediments were used within 24 h of collection. One aquarium was set up for each sediment type, with sediment layering as in the field. The most permeable sediment was brownish throughout the upper 20 cm and did not show this conspicuous layering. Nevertheless the aquarium was prepared in the same way. To avoid air bubbles, aquaria were filled with seawater before sediment was added. Visible animals in the sediment were removed. After filling the bottom of the aquaria with the gray sediment, nets (1-mm mesh) were placed onto the gray sediment to prevent lugworms from inhabiting the edges of the aquaria, and then the remaining sediments were added. Newly filled aquaria were left to settle for at least 12 h under continuous flow of aerated seawater over the sediment surface before individual specimens of *A. marina* were added. The added lugworms had a mean wet weight of 11.4 g (SD = 3.7 g), a mean length of 17.8 cm (± 2.3 cm), and a mean width of 1.1 cm (± 0.1 cm). They were allowed to establish themselves in the sediments for 48 h prior to measurements. During measurements the seawater (salinity of 32‰) above the sediment surface was exchanged continuously at a rate of ~ 10 mL min^{-1}, and the aquaria were kept in the dark at 15°C.

Sediment characterization—For each sediment type, three polyvinyl chloride (PVC) cores (10 cm^2, 20 cm length) were filled with sediment in the same way as the sandwich aquaria and used for the determination of porosity, total organic matter (loss on ignition at 450°C for 8 h), and hydraulic conductivity (constant pressure head) (Klute and Dirksen 1986).

Porewater pressure recording—Porewater pressure dynamics associated with the biohydraulic activity of the lugworm were detected with pressure sensors (Measurement Specialties Model 86, 34.5 kPa, stainless steel diaphragm) sampling at a frequency of 40 Hz. The sensors were calibrated by immersion in eight known water depths from 0 to 14 cm ($r^2 > 0.995$) and deployed through threaded holes in the center of the transparent aquarium wall. The sensors detect pressure fluctuations around the hydrostatic baseline, which depends on the depth of the pressure sensor below the water surface. According to Darcy's law, the porewater pressure is basically a function of the instantaneous pumping rate, the volume of the sediment over which porewater flow occurs, the distance between the pressure source and the sensor, and the permeability of the sediment. Because of the constraints imposed by the aquarium wall, the detected porewater pressures may have been amplified relative to the unconstrained geometry. However, we primarily used the temporal variations of the pressure transients to identify the type of biohydraulic activity, and these have been shown not to depend on the geometry employed (Wethey et al. 2008).

Time-lapse imaging—Photographs of the sediment, taken through the transparent wall every 30 s using a digital camera (1936 × 1296 pixels, effective pixel size of 0.24 mm) with flash, were used for the identification of the sediment surface, sediment reworking, and behavioral analysis. The behaviors were identified and classified as described previously (Wethey et al. 2008; Woodin and Wethey 2009). Since all recording instruments were synchronized, it was possible to correlate lugworm behaviors with their effects on porewater pressure dynamics and sediment oxygenation. Predictions of behaviors based on the pressure data were cross-checked against the optode data and vice versa.

Oxygen dynamics and oxygen consumption rates—Effects of lugworm activity on the O_2 dynamics and water flow in and above the sediment were characterized using the O_2 imaging technique (Polerecky et al. 2006). One side of each aquarium was equipped with a semitransparent O_2 sensitive optode (30 × 20 cm), which was constructed by knife-coating a mixture of polystyrene, a Pt-porphyrine dye and TiO_2 particles dissolved in chloroform onto a polyethylene terephthalate (PET) support foil (Precht et al. 2004). O_2 images at this wall were taken with a luminescence lifetime imaging system (Holst and Grunwald 2001; *see* also www.microsen-wiki.net). The optode was calibrated using luminescence lifetime values measured in the anoxic sediment and air-saturated seawater (Kühl and Polerecky 2008). To reduce noise, 2 × 2 pixels of the images were binned, resulting in an effective pixel size of 0.56–0.59 mm. O_2 images were recorded in 15-s intervals over at least 48 h for each studied sediment type.

At the end of the long-term O_2 dynamics measurements, 5 mL of air-saturated seawater was carefully injected with a syringe to a depth of ~ 10 cm near the optode. Afterward, oxygen images were recorded every 15 s, and those acquired during periods of little or no porewater movement were used to estimate sedimentary O_2 consumption rates (OCR, in mol O_2 m^{-3} min^{-1}). First, an image of OCR (covering an area > 1 cm^2, i.e., > 350 pixels) was calculated by multiplying the initial rates of decrease in O_2 concentration by the sediment porosity for every pixel (Polerecky et al. 2005). Subsequently, the median, mean, and standard deviation OCR values for this area were calculated. Since the aerated seawater was injected into previously not oxygenated sediment, this gave an estimate of the maximum OCR, i.e., with contributions of both biotic and abiotic oxygen consumption.

Data analysis—A number of approximations were made to be able to extract quantitative information from the oxygen images. Because of the constrained geometry, the results obtained may not accurately represent the situation in unconstrained sediments (*see* Discussion). However, the calculations are useful for the understanding of the magnitude of the effects that lugworm biohydraulic activities induce in different sediment types. In our analysis, oxygenated sediment was defined as sediment where the detected porewater O_2 concentrations were above 5% air saturation (AS). Analysis was done in Matlab (version 7, Mathworks; utilities available from authors). The pressure sensor data were used to confirm directionality, frequency, and type of hydraulic behaviors. These parameters are known to be comparable for individuals in unrestrained sediments and sandwich aquaria such as used here (Wethey et al. 2008).

The volume of oxygenated sediment at depth at any given time, V_{O_2deep}, was estimated by assuming that the oxygenated porewater moved concentrically away from the injection point to fill the volume of a sphere whose caps on both ends are cut off by the aquarium walls (Fig. 1A). Based on this approximation, one oxic pixel on the optode corresponds to $V_{O_2deep} \approx 0.9$ cm^3 in the sediment. To avoid overestimation of V_{O_2deep} due to the pixel noise in the data, we conservatively set V_{O_2deep} to 0 cm^3 for areas of 3 × 3 pixels (~ 0.03 cm^2) and below, even though the true oxygenated sediment volume was somewhere between 0 and 0.94 cm^3.

The volume of the oxygenated surficial sediment, $V_{O_2surface}$, was estimated as $2d\ A_{O_2surface}$, where $A_{O_2surface}$ is the area of oxygenated sediment detected on the optode that was immediately below the sediment–water interface. The exact position of the sediment surface was identified from direct imagery. The infiltration of oxic water into the surficial sediments is not comparable to an injection into the subsurface sediment, which expands in all directions. Thus we used a rectangular solid for this calculation and assumed that the vertical O_2 penetration depth into the surficial sediments, as detected by the optode at a given horizontal position, was constant throughout the vertical plane perpendicular to the aquarium wall. The mean oxygen penetration depth (OPD) was calculated as $V_{O_2surface}/A$, where A is the surface area of the sediment in the aquarium.

The potential diffusive O_2 penetration depth (DOPD) into the surficial sediment in the absence of bioadvection

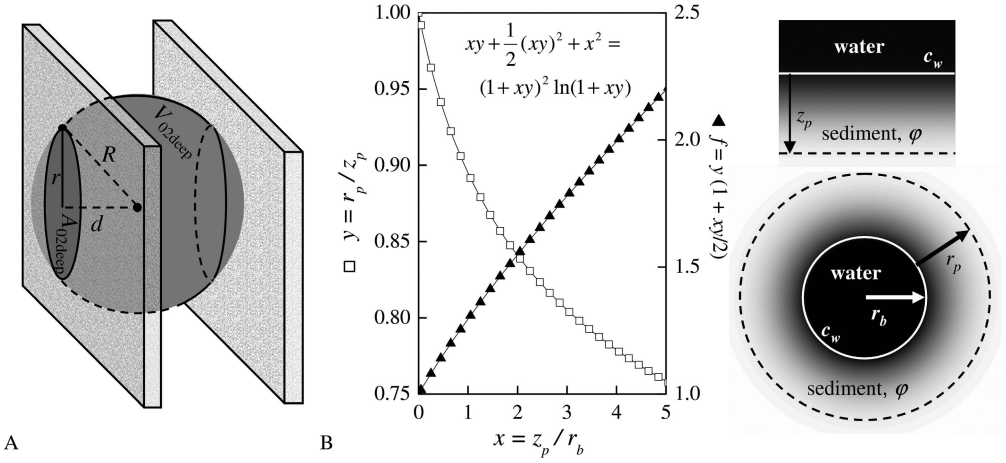

Fig. 1. (A) Approximation of the oxygenated sediment volume by a sphere whose caps are cut off on both sides by the aquarium walls. This volume is given by $V_{O_2deep} = \frac{4}{3}\pi R^3 - \frac{1}{3}\pi(R-d)\left[3r^2+(R-d)^2\right]$, where d is the distance from the injection point to the aquarium walls, here assumed to be equal to the half of the aquarium width (here d = 0.6 cm), and $R=\sqrt{r^2+d^2}$. Although the oxygenated sediment area detected by the optode, A_{O_2deep}, was not perfectly circular, r was estimated assuming that it was, i.e., $r=\sqrt{A_{O_2deep}/\pi}$. (B) The relationship between the diffusive O_2 penetration distance under planar (z_p) and cylindrical (r_p) geometry, derived by solving steady state diffusion equation $0 = D_s\nabla^2 c - OCR$ in the respective geometries, where D_s is the O_2 diffusion coefficient and OCR is the O_2 consumption rate, both in sediment of porosity φ. Assuming zero-order kinetics, homogeneous OCR and D_s throughout the sediment, and a fixed O_2 concentration at the sediment–water interface ($c = \varphi c_w$, where c_w is the O_2 concentration in water), the solution leads to an implicit equation between dimensionless parameters $x = z_p/r_b$ and $y = r_p/z_p$ shown in the inset, where r_b is the burrow radius and $z_p = (2D_s\varphi c_w/OCR)^{1/2}$. Graph shows the numerically calculated $y(x)$, as well as the factor $f(x)$ that is used to calculate diffusive oxygen uptake (DOU) by the sediment surrounding the burrow from the expression $DOU = A_{burrow}\,OCR\,fz_p$, where $A_{burrow} \approx (2\pi r_b L + \pi r_b^2)$ is the approximate area of a blind-ending burrow of length L and radius r_b.

was estimated from Fick's law of diffusion. Assuming depth-independent OCR and zero-order kinetics, DOPD was calculated as $z_p=\sqrt{2D_s\varphi c_w/OCR}$, where c_w is the O_2 concentration in the overlying water (here c_w = 258.8 μmol L^{-1}, corresponding to 100% AS), D_s is the effective diffusion coefficient of O_2 in the sediment. D_s was calculated as $(\varphi/\theta^2)D_w$, where $D_w = 1.715 \times 10^{-5}$ cm^2 s^{-1} is the diffusion coefficient of O_2 in water corrected for the experimental salinity and temperature (Jørgensen and Revsbech 1985), φ is the sediment porosity, and θ is tortuosity approximated as $\theta^2 = 1 - \ln(\varphi^2)$ (Boudreau 1996). Because our estimates of DOPD were based on the OCR measured at depth (*see* above), these values should be interpreted as crude approximations for O_2 penetration into the surficial sediment, because the OCR in surface sediments are very likely lower and thus oxygen would penetrate deeper.

Temporal patterns in lugworm activity were investigated by plotting V_{O_2deep} as a function of time and measuring the period, i.e., the time interval (T_{per}) between the beginning of an increase in V_{O_2deep} and the beginning of the subsequent increase. This was done for all detected oscillations in V_{O_2deep}. In less permeable sediments, where the lugworm's activity did not always result in deep sediment oxygenation visible at the optode, we instead calculated the area of suboxic plumes emerging above the sediment surface and used the temporal variations of this area to characterize the activity patterns and calculate T_{per}. The activity cycles derived from optode imagery were compared to synchronous pressure records (magnitude, frequency, and directionality of pressure pulses) and visible-light imagery to confirm patterns.

The instantaneous pumping rates (R_p, in milliliters per minute) were estimated using the expansion and decline of the oxygenated sediment volume V_{O_2deep}. A conservative estimate was obtained by assuming that the observed increase in V_{O_2deep} (Fig. 1A) was caused by the replacement of anoxic porewater with oxic overlying water (oxygen concentration c_w) that was pumped into the sediment by the lugworm. Additionally, we corrected for sedimentary O_2 consumption by considering that oxygen in the volume V_{O_2deep} must be replenished at a rate equal to its consumption, i.e., OCR V_{O_2deep}/c_w, to maintain a constant value of V_{O_2deep}. Thus, the pumping rates were approximated as

$$R_p = \varphi\frac{\partial V_{O_2deep}}{\partial t} + \frac{OCR}{c_w}V_{O_2deep} \quad (1)$$

When V_{O_2deep} decreased faster than would be expected solely from oxygen consumption in the sediment, this approach predicted negative flow rates, i.e., pumping of water out of

the burrow (and the surrounding sediment) through the open tail shaft into the overlying water. The pumping direction derived from O_2 imaging was verified with that predicted from the pressure sensor data.

This approach only allowed the detection of negative flow rates when O_2 was present at the optode at the beginning of a backward pumping period. We therefore applied an alternative approach to estimate the instantaneous pumping rates, which was based on the emergence and disappearance of anoxic water as visualized on the optode above the sediment surface. This gave, however, only very rough estimates, because the presence of oxygen depended not only on the ascent and descent of suboxic and anoxic water but also on the mixing with overlying circulating oxic water, which was not possible to quantify by our methods.

The movement of suboxic fronts detected by the optode was used to estimate the velocities of the water flow at the aquarium wall induced by the hydraulic activity of the lugworm. This was done by evaluating the displacement of O_2 contour lines in time in the direction perpendicular to the contour line. "Smearing" of the O_2 fronts due to diffusion was ignored, since it was negligible compared to the advective transport. For the volume above the sediment–water interface, this calculation gave an estimate of velocities of water flowing out of the sediment. For the most permeable sediment, we also applied this calculation to deeper sediment layers, where the suboxic fronts moved approximately concentrically away and toward the lugworm. For simplicity, the effects of sedimentary OCR and turbulent mixing in the overlying water were not considered; thus our estimates are conservative.

Redox oscillations in the sediment were characterized using the sequence of intervals during which the sediment experienced oxic (T_{ox}) and anoxic (T_{anox}) conditions. A single redox oscillation was defined as the duration between two subsequent oxic–anoxic cycles, i.e., $T_{redox} = T_{anox} + T_{ox}$. The complete T_{ox} series was summed and divided by the measurement duration (48 h) for every pixel of the optode, giving a two-dimensional (2D) map of sediment oxygenation probability, $P(O_2 \geq 5\%)$. Furthermore, the values of T_{redox}, T_{anox}, and T_{ox} were averaged for every pixel, giving a 2D map of the average redox oscillation period and the average duty cycle ($T_{ox} : T_{redox}$). These quantities were calculated only for pixels with detectable redox oscillations.

Oxygen budgets for each lugworm and sediment combination were evaluated assuming that oxygen pumped in the tail-to-head direction into the burrow and feeding pocket was consumed by (1) respiration by the worm, (2) diffusive transport across the burrow wall, and (3) oxygen consumption in the advective zone surrounding the burrow. Respiration rate of an individual lugworm was taken as $LR = 1$ μmol O_2 h^{-1} per gram wet weight at 15°C (Wittmann et al. 2008). For estimations of the diffusive O_2 uptake across the burrow wall, we assumed a blind-ending cylinder with a radius of $r_b = 0.5$ cm and a length of L, which ranged between 25 and 38 cm, as determined by visual imagery. The surface area of the burrow was estimated as $A_{burrow} = 2\pi r_b L + \pi r_b^2$, thus roughly 80–120 cm^2. This is two to threefold larger than areas reported in previous studies (Meysman et al. 2005; Timmermann et al. 2006), but reasonable, since the lugworms in our study had approximately twofold greater wet weight and diameter. The diffusive O_2 uptake (DOU) was then estimated as $DOU = A_{burrow}$ OCR f z_p, with z_p (in cm) and OCR (in μmol cm^{-3} s^{-1}) obtained as described above. The factor f was calculated as described in Fig. 1B. For the assumed burrow radius $r_b = 0.5$ cm and the estimated range of z_p, f ranged from 1.03 to 1.06. The advective O_2 uptake (AOU) was estimated as $AOU = V_{O_2 deep}$ OCR. Based on the estimated total O_2 uptake ($TOU = LR + DOU + AOU$), we calculated the time-averaged pumping rates required to provide this total O_2 flux as $TOU : c_w$, assuming air-saturated O_2 concentration ($c_w = 258.8$ μmol L^{-1}) in the pumped water. These calculations pertain only to periods when the worm is pumping in the tail-to-head direction and thus are comparable to those of other authors. We did not do the parallel calculation for when the worm is pumping in the head-to-tail direction because we do not have an OCR value for surficial sediments where organic sources are likely to be richer and reduced inorganic compounds less abundant than at depth.

Results

The sediments, all inhabited by the lugworm *A. marina*, ranged from highly permeable coarse sand to low-permeability muddy sand with hydraulic conductivities between 3.3 and 0.1 cm min^{-1}, respectively (Table 1). They all had low organic content ($< 1\%$ dry weight) and similar porosity (~ 0.4). The sedimentary OCRs varied inversely with hydraulic conductivity, with the median values increasing by a factor of ~ 3.3 between the high- and low-permeability sediments (Table 1).

Diverse lugworm activities induced characteristic porewater pressure waveforms above and below the hydrostatic baseline (Fig. 2). Peristaltic pumping induced periodic pressure oscillations at typical frequencies of 1.5–4 min^{-1}. Burrowing sequences were characterized by larger positive and negative pressure spikes occurring typically in 2-min intervals accompanied by higher frequency and lower magnitude positive or negative oscillations (Fig. 2B,E). Defecation events were associated with a massive but short (6–10 s) negative pressure pulse followed by a short period of higher frequency (~ 5 min^{-1}) pressure pulses above baseline (Fig. 2B,E) (Woodin and Wethey 2009). The magnitude of the pressure oscillations varied inversely with sediment permeability (Fig. 2B), while the behavior-specific shapes of the pressure waveforms were similar for all sediments.

Simultaneous oxygen and pressure measurements revealed that the pressure oscillations associated with each hydraulic activity induced characteristic bioadvection and oxygenation within the sediment and in the overlying water. The spatiotemporal dynamics of bioadvection varied considerably among the investigated sediment types (Fig. 2; Tables 1 and 2; and Web Appendix, Videos 2–4).

In the most permeable sand with the lowest sedimentary OCR (Table 1), hydraulic activities that pressurized the

Table 1. Characteristics of the studied sediments and quantities estimated for the sediments from oxygen imaging measurements. Total organic content (TOC) is given in percentage of dry weight of sediment, sedimentary oxygen consumption rates (OCR) are given both per volume of porewater (μmol L^{-1} min^{-1}) and per volume of sediment (i.e., grains plus porewater; μmol cm^{-3} h^{-1}). V_{O_2deep} denotes oxygenated sediment volume at depth, $V_{O_2surface}$ is the volume of oxygenated surficial sediment, OPD denotes the observed oxygen penetration depth, and DOPD is the oxygen penetration depth estimated based on diffusive transport. Sediments listed from highest to lowest permeability.

Permeability	10^{-12} m^2	mean	59	32	28	20	8.9	1.6
Hydraulic conductivity	cm min^{-1}	mean	3.3	1.8	1.5	1.1	0.5	0.09
		SD	0.2	0.03	0.2	0.2	0.1	0.01
Porosity	% volume	mean	0.43	0.40	0.40	0.393	0.40	0.39
		SD	0.01	0.01	0.02	0.004	0.01	0.01
TOC	% weight	mean	0.35	0.27	0.29	0.32	0.44	0.74
		SD	0.13	0.03	0.04	0.03	0.05	0.09
OCR	μmol L^{-1} min^{-1}	median	11	19	21	23	43	37
	μmol cm^{-3} h^{-1}	median	0.29	0.46	0.51	0.55	1.03	0.88
	μmol L^{-1} min^{-1}	mean	13	26	22	25	52	45
	μmol L^{-1} min^{-1}	SD	11	21	13	12	30	27
V_{O_2deep}	cm^3	max	278	41	37	60	15	7
		mean	114	5.1	5.4	10.7	1.7	1.1
		SD	59	6.2	5.6	9.3	1.6	1.2
$V_{O_2surface}$	cm^3	max	92	48	17	6.1	9.0	10.1
		mean	21	11	2.3	1.1	1.4	1.2
		SD	25	6.6	2.1	0.9	1.6	1.0
OPD	cm	max	2.6	1.3	0.5	0.2	0.3	0.3
		mean	0.60	0.31	0.06	0.03	0.04	0.03
		SD	0.69	0.18	0.06	0.02	0.04	0.03
DOPD	cm		0.09	0.06	0.06	0.06	0.04	0.04

sediment resulted in persistent sediment oxygenation at depth, with oxygenated areas continuously varying in size and shape (Figs. 2A, 3A, left panels; Web Appendix, Video 2). Over 48 h, on average 113 cm^3 of the sediment was oxygenated with concentrations of typically $<$ 20% air saturation (AS) at the aquarium wall (Table 1, V_{O_2deep}). Suboxic fronts moved in an approximately concentric manner, with typical velocities of $\sim$ 2 mm min^{-1} at the aquarium wall 3–5 cm away from the worm. During periods of intensive pumping, the oxygenated sediment volume increased by $\sim$ 120 cm^3 in less than 20 min, suggesting pumping rates of $\sim$ 2.5 mL min^{-1} averaged over 20 min. During such periods oxygen concentrations at the aquarium wall occasionally increased above 40% AS. However, increases in the volume of deep oxygenated sediment were observed even during periods with small pressure pulses (e.g., time interval between 2.5 and 3.5 h in the left panel of Fig. 2B,D). This indicated that the advective transport in the sediment was driven also by comparatively small but continuous pressure oscillations of the peristaltic pumping by the lugworm. Simultaneously with the emergence of subsurface oxic regions, suboxic or anoxic porewater exited through the sediment–water interface approximately homogeneously over the entire width of the aquarium as a flow "sheet," indicating even percolation of this sediment in the vertical direction over almost the entire constrained surface of 36 cm^2 (Fig. 3A; Web Appendix, Video 2). The suboxic front ascended with velocities of 0.5–1 mm min^{-1} during intensive pumping periods.

In the intermediate and low-permeability sediments, the spatial extent of sediment oxygenation was considerably smaller (Table 1, V_{O_2deep} and $V_{O_2surface}$; Figs. 2A,D, 3B,C, middle and right panels), presumably because of higher OCR in sediments with lower hydraulic conductivities (Table 1). Oxygen (typically at concentrations below 20% AS) reached the aquarium wall only during periods of intense activity and disappeared rapidly when the activity ceased (Figs. 2D, 3B,C; Web Appendix, Video 3). Hydraulic pressurization by peristalsis at depth, as detected by the pressure sensors, coincided with the appearance of concentrated suboxic plumes at and above the entire sediment surface, indicating localized leakage of porewater from the sediment to the overlying water (Figs. 2, 3B,C; Web Appendix, Video 3). Suboxic and anoxic porewater ascended into the overlying water with velocities of about 4 mm min^{-1}, 4–8 times faster than the movement of the suboxic or anoxic sheet exiting the highly permeable sediment. Negative pressure pulses, detected by the pressure sensors and associated with burrowing and defecation by the lugworms, resulted in a temporary collapse of these plumes (Fig. 2B,C).

Porewater bioadvection induced by the hydraulic activity of the lugworm was clearly not unidirectional. In addition to the transient flow reversals, such as those induced by short negative pressure pulses during burrowing and defecation, we also observed longer periods (up to 20 min) of active reversed pumping, sometimes but not always in combination with burrowing pressure spikes (Figs. 2B,E, 4). The porewater pressure during these reverse pumping periods fell below hydrostatic baseline and induced intense percolation of the overlying water into the sediment through the sediment–water interface (Figs. 2C, 4E). This occurred almost over the entire surface of the aquarium and led to an increase in the oxygen penetration depth from a few millimeters during low

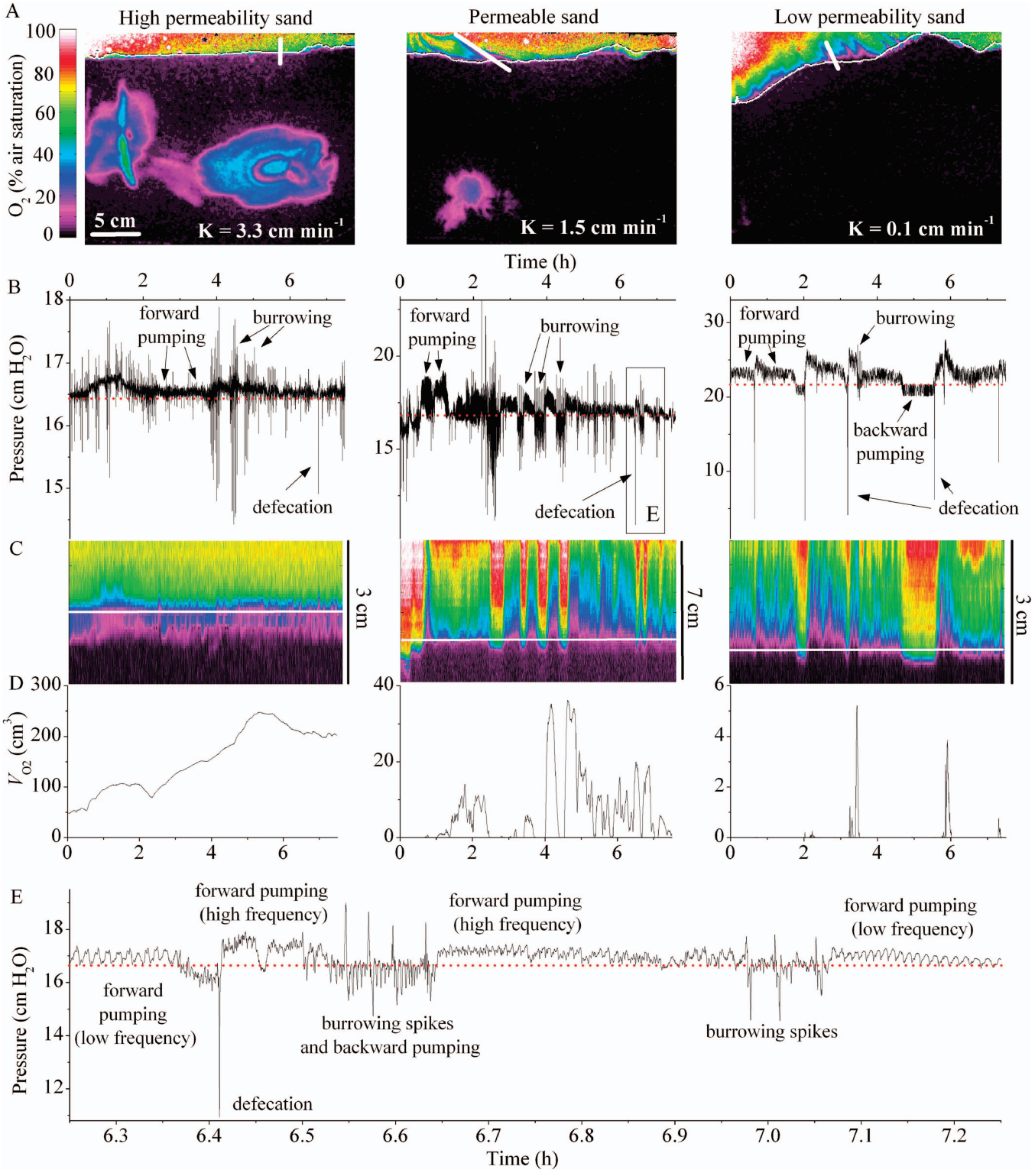

Fig. 2. Hydraulic activities, pressure transients, and related oxygen dynamics in three sediment types with different hydraulic conductivities (*K*). (A) Shown are exemplary optode images of oxygen distributions, (B) time series of behavior-specific pressure transients, (C) oxygen concentrations in selected profiles across the sediment–water interface, and (D) volumes of subsurface oxygenated sediment. (B–D) are isochronal with one another, while the exemplary images shown in panel A correspond to time points 5.3 h, 4.1 h, and 2.2 h from left to right. (E) shows an expansion of the indicated section of panel B. Solid lines in panel A indicate the positions of the profiles for which time series are shown in panel C. White horizontal line in panels A and C indicates the sediment surface. Red dotted horizontal lines in panels B and E indicate the hydrostatic baseline of porewater pressure.

Table 2. Oxygen budgets in the studied sediments, estimated based on the data in Table 1 and expressed as uptake rates mediated by an individual lugworm as well as in percentage of the total flux. Lugworm respiration rates are from Wittmann et al. (2008). The lugworm-mediated O_2 uptake is based on the assumption of 30 individuals m^{-2} with comparable rates of activity.

Permeability	10^{-12} m^2	59	32	28	20	8.9	1.6
Advective O_2 uptake	μmol h^{-1}	32.6	2.3	2.8	5.9	1.7	1.0
Diffusive O_2 uptake	μmol h^{-1}	2.1	2.6	3.8	3.5	4.3	4.5
Lugworm respiration	μmol h^{-1}	5.7	9.1	11.4	11.4	15.3	15.5
Total O_2 uptake	μmol h^{-1}	40.4	14.0	18.0	20.8	21.3	20.9
Average pumping rates	mL $ind.^{-1}$ min^{-1}	2.6	0.9	1.2	1.3	1.4	1.3
Advective O_2 uptake	%	81	17	15	28	8	5
Diffusive O_2 uptake	%	5	19	21	17	20	21
Lugworm respiration	%	14	65	63	55	72	74
Lugworm-mediated O_2 uptake	mmol m^{-2} d^{-1}	29.1	10.1	13.0	15.0	15.4	15.1

activity to, depending on the sediment, up to several centimeters (Table 1, OPD; Fig. 4E; Web Appendix, Video 4). Flow reversals were also reflected in concentric transport of suboxic and anoxic porewater toward the lugworm, causing rapid collapse of the subsurface oxic volume (Fig. 3A, profile A2, minutes 20–30 and 60–65; Fig. 3B, profile B2, minutes 20–30; Web Appendix, Video 2). They also resulted in the appearance of large suboxic or anoxic fountains that ascended from the tail shaft into the overlying water (Fig. 4C,D; Web Appendix, Video 4). In low-permeability sediments with high OCR, where oxic water reached the optode in the subsurface sediment only rarely (Fig. 2D), flow reversals were detected by the appearance of suboxic fountains ascending from the tail shaft as described above. In addition, suboxic plumes exiting the sediment surface during forward pumping collapsed when the pumping was reversed and the overlying water penetrated into the surficial sediments resulting in OPD values in excess of those predicted for diffusion (Fig. 3C, profile C1, minutes 40–55, 90–105, 135–140; Table 1, OPD vs. DOPD).

Diffusive oxygen penetration depths (DOPDs) estimated based on the diffusive transport varied between 0.4 and 0.9 mm across the studied sediment types (Table 1). These DOPDs were at the lower range of OPD that we observed in aquaria with comparable sediments without lugworms present, suggesting an underestimation of the DOPD into the surficial sediment based on OCR estimated for deeper sediments. In all sediments underpressurization of the sediment resulted in a 2- to 12-fold larger OPD than would be expected from diffusion alone (Table 1, OPD vs. DOPD). In the intermediate and low-permeabilty sediments, the time-averaged OPDs were in the same range as the estimated DOPD, reflecting the fact that the increased oxygen penetration during underpressurization was equalized by the upward transport of anoxic porewater and the resultant elevation of the oxic–anoxic boundary above the sediment surface during pressurization. Overall, the assumed constant

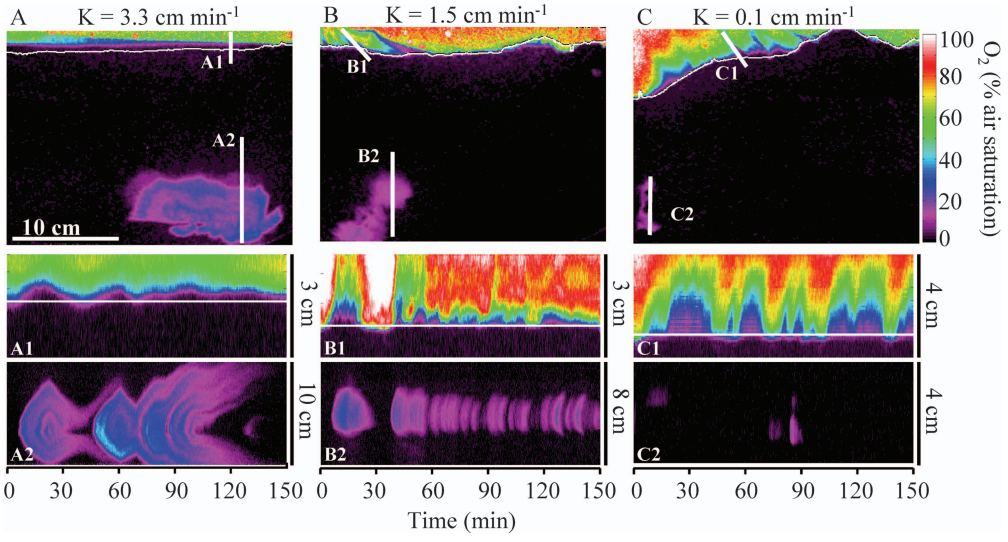

Fig. 3. Exemplary oxygen optode images (top panels) and isochronal time series of profiles of oxygen concentrations (bottom panels) demonstrating sediment-specific patterns of porewater flow out of the sediment induced by biohydraulic pressurization. Positions of the profiles are indicated by thick white lines in the top panels, one intersecting the sediment–water interface parallel to the apparent path of anoxic water escaping from the sediment, the other one located deep within the sediment parallel to the main vertical sediment axis. Thin white solid lines depict the sediment surface. *See* also Web Appendix, Video 2 and 3 for the corresponding O_2 dynamics.

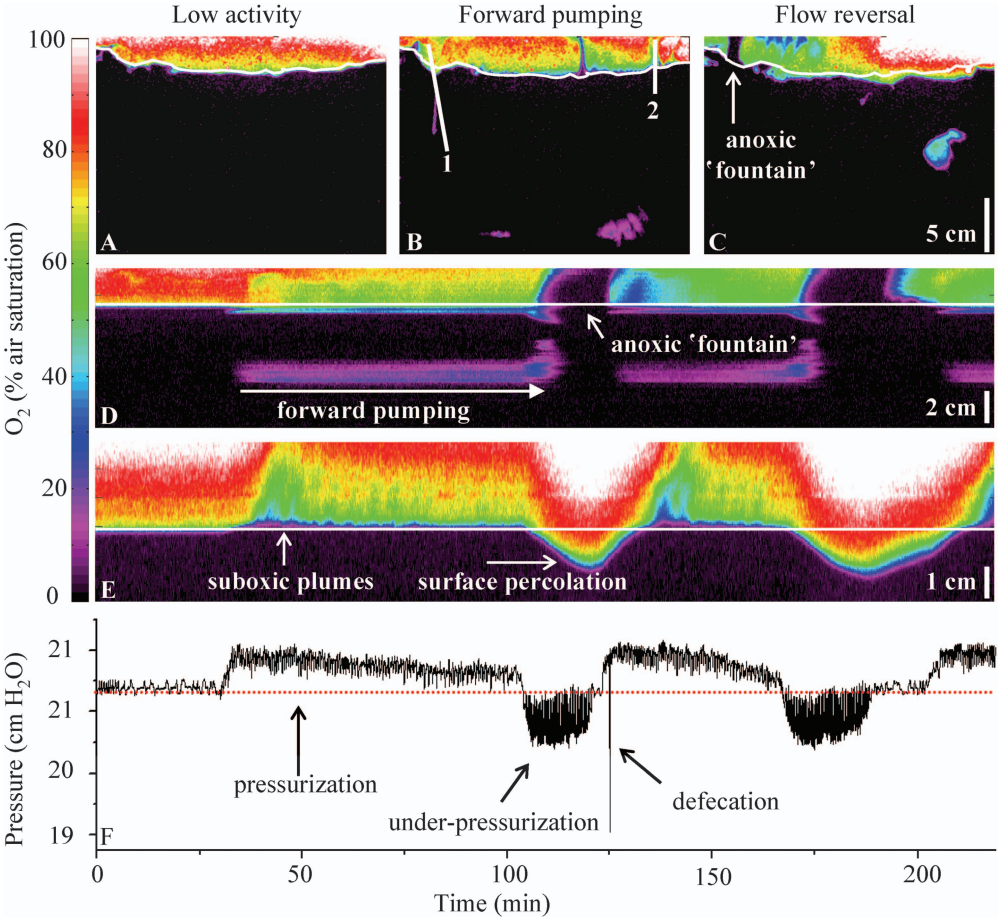

Fig. 4. Oxygen images and time series of profiles of oxygen concentrations demonstrating flow reversals and oxygenation of surficial sediments induced by biohydraulic underpressurization. Shown are (A) exemplary oxygen images during a sequence of low lugworm activity, (B) repeated forward, and (C) reversed pumping, and time series (~ 3.5 h long) of oxygen concentrations in selected profiles close to the tail shaft (D, profile 1) and above the feeding pocket (E, profile 2). Profile positions are marked by lines 1 and 2 in panel B. (F) shows the corresponding pressure record. (D–F) are isochronous. White solid lines in panels A–E indicate the sediment surface; red dotted line in panel F indicates the hydrostatic baseline pressure. *See* also Web Appendix, Video 4 for the corresponding O_2 dynamics.

DOPD in the absence of hydraulic activity contrasted dramatically with the highly dynamic and variable OPD observed when lugworms were active (Figs. 2–4), as indicated by large standard deviations relative to the mean of the OPD values averaged over 48 h (Table 1).

Pumping rates, estimated from the wax and wane of the subsurface oxygenated volume and the emergence of suboxic or anoxic plumes above the sediment surface, were highly variable in magnitude and direction and closely linked to the independently measured fluctuations in porewater pressures (Fig. 5). Only in sediments of intermediate hydraulic conductivity could pumping rates be determined both from the expansion and contraction of oxic areas detected by the optode at depth and from the temporal dynamics of suboxic or anoxic plumes emerging from the sediment surface, and these two estimates agreed reasonably well with one another and with the pressure sensor data. The rates ranged between 1 and 2 mL min^{-1} for forward peristalsis, with occasional transient peaks of > 5 mL min^{-1} (Fig. 5). Pressure pulses below the hydrostatic baseline during burrowing and defecation were accompanied by backward pumping at typical (negative) rates of 1–2 mL min^{-1}, with occasional peaks of 5 mL min^{-1} (e.g., in intervals 23–38 and 153–158 min in Fig. 5).

In the most permeable sediment the pumping rates, estimated from the dynamic oxygenation at depth, were typically around 4 mL min^{-1}, with occasional peaks of up to 8 mL min^{-1} during forward pumping. The estimates based on synchronous emergence of suboxic or anoxic water as a sheet above the sediment surface were lower (1 mL min^{-1} or less), possibly because of the mixing of the ascending suboxic or anoxic porewater with the oxygenated overlying water, which could not be accounted for by our method. The opposite was true for the low-permeability sediment; instantaneous pumping rates estimated from the emerging suboxic or anoxic water above the sediment varied between 1 and 3 mL min^{-1}, whereas those calculated from the subsurface sediment oxygenation were much

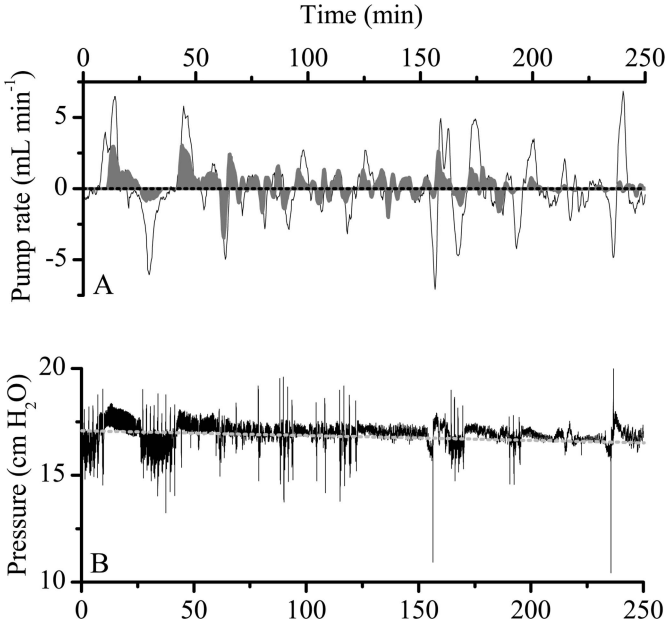

Fig. 5. (A) Pumping rates of the lugworm *A. marina* in a sediment of intermediate hydraulic conductivity (1.5 cm min^{-1}), estimated from the temporal dynamics of oxygenated sediment volume at depth (gray shaded area) and suboxic plumes emerging at the sediment surface (black line) using Eq. 1. (B) The synchronously detected dynamics of porewater pressure fluctuations, with the horizontal black and white line indicating the hydrostatic pressure baseline. Porewater pressure pulses above and below hydrostatic baseline coincided with positive and negative pumping rates derived from O_2 dynamics. However, intervals of active pumping detected in the pressure records as well as by the emergence of suboxic plumes above the sediment surface were sometimes not detected in the deep sediment oxygenation record, presumably because of a combination of hydraulic conductivity restrictions and sedimentary oxygen demand (e.g., during intervals 20–40 min or 190–250 min).

lower (< 0.6 mL min^{-1}). This discrepancy was possibly a result of the combination of high sedimentary oxygen consumption and low permeability, which limited the pumped oxygenated water in reaching the optode and thus led to underestimated V_{O_2deep}.

Over the 48 h of observation, the sediment volume that was intermittently supplied with oxygen, as well as the relative length of these oxygenation events, varied strongly among the sediment types (Figs. 6, 7). The sediment area that experienced oxygen for at least 1 min during 48 h was positively correlated with the sediment permeability ($r^2 = 0.910$, $p \leq 0.003$). In the most permeable sediment with the lowest OCR, $\sim$ 83% of the sediment in contact with the optode was oxic ($>$ 5% AS) for at least 1 min of the 48 h, with more than 50% of this area being oxic for more than 10% of the time (Fig. 7A). The area that experienced oxic–anoxic oscillations decreased to less than 4% in the sediment with the lowest permeability, and the probability of the presence of oxygen was typically less than 5% for most of this area. In the intermediate- and low-permeability sediments, areas with higher oxygenation probabilities ($>$ 10%), were restricted to zones close to the feeding pocket and the gallery or to the tail shaft (Fig. 6).

Sedimentary oxygen dynamics induced by the hydraulic activities of the lugworms were variable but followed a consistent temporal pattern. Based on the wax and wane of oxygenated areas at depth and/or the emergence and collapse of anoxic or suboxic plumes above the sediment surface, the average intervals between subsequent periods of sediment pressurization and the associated porewater advection ranged between 17 and 37 min for all sediments (Fig. 7B, T_{per}). This activity pattern was confirmed by the quantification of redox oscillations, which was done for every pixel of the optode below the sediment surface. The durations of redox oscillations, i.e., transitions from oxic to anoxic conditions and back (T_{redox}), varied substantially among pixels (15–45 min), but the averages over pixels that experienced redox oscillation were similar for all investigated sediments (25–35 min; Fig. 7B). In contrast, the durations of the oxic intervals in the redox oscillation, T_{ox}, were significantly positively correlated with sediment permeability ($r^2 = 0.843$, $p \leq 0.01$) and increased from 3 to 12 min between the lowest and highest permeability sediment (Fig. 7B). Thus, the average oxic "duty cycle" of the redox oscillations increased from 10% to 40% as a function of the sediment type.

The estimated relative contributions of lugworm respiration, diffusive uptake across the burrow walls, and uptake in the zone percolated by porewater bioadvection to the overall oxygen budget varied dramatically among the investigated sediment types (Table 2). In the intermediate sediments, about half of the oxygen pumped into the burrow was consumed by lugworm respiration, while the worms' efficiency in using the pumped oxygen for respiration was higher in the low-permeability sediments and much lower in the highly permeable sand. The diffusive O_2 flux over the burrow wall accounted for about 20% of the total O_2 uptake in all sediments, except for the highly permeable sand, where advection was by far the dominating mechanism of O_2 transport (Table 2). In the sediments with intermediate permeabilities the diffusive and advective oxygen flux contributed equally or within less than a factor of two to the overall O_2 flux from the burrow into the surrounding sediment. However, this O_2 transport was dominated by diffusion ($>$ 80%) in low-permeability sediments and by advection in the highly permeable sand ($>$ 90%).

The time-averaged lugworm pumping rates derived from the estimated total O_2 uptake from the overlying water amounted to $\sim$ 2.6 mL min^{-1} for the most permeable sediment, while the values were lower but similar (0.9–1.4 mL min^{-1}) in the other sediment types. These estimates were in the same range as the time averages of instantaneous pumping rates derived from the changes in the volume of oxygenated sediment at depth or changes in the volume of suboxic or anoxic water exiting the sediment (Fig. 5).

Discussion

As has been demonstrated repeatedly for a variety of benthic infauna, behavioral activities are not equivalent in duration or frequency (Jumars and Wheatcroft 1989; Pearson 2001; Rosenberg 2001). This is clearly true for

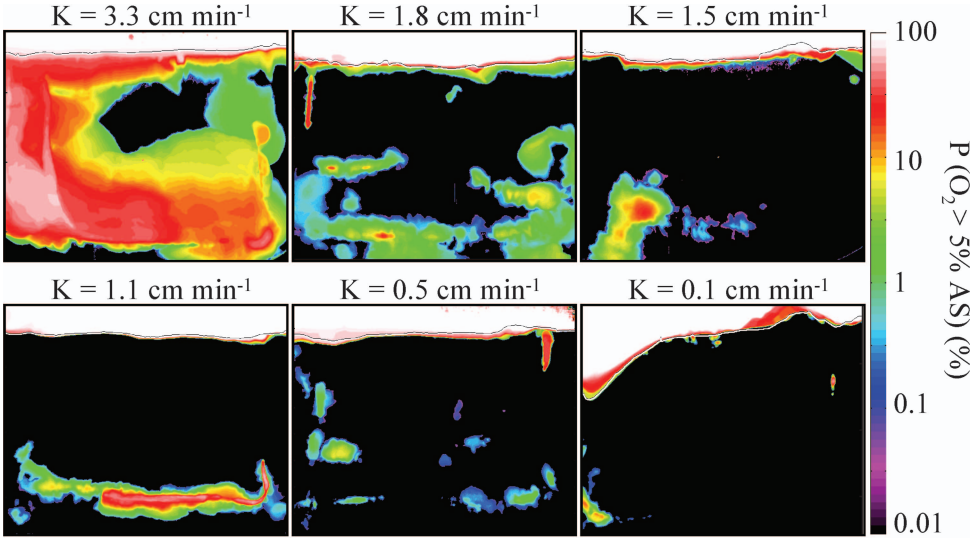

Fig. 6. Probability distribution of the presence of oxygen ($O_2 > 5\%$ air saturation) at the aquarium wall during 48 h of measurements, plotted in color-coded logarithmic scale for the studied sediment types (hydraulic conductivity given in legend and color code for oxygen values on far lower right). Thin black line indicates the sediment surface. Certain areas above the sediment surface have values lower than 100% (e.g., for sediment with $K = 0.1$ cm min^{-1}) as a result of movement of the sediment surface during the measurement period as a result of sediment subduction and creation of the fecal mound by the lugworm. Areas that were anoxic during the entire measurement are shown in black.

arenicolid polychaetes, which perform a variety of behaviors that transport sediment particles and porewater (Riisgård and Banta 1998; Timmerman et al. 2006; Woodin and Wethey 2009). The goal of this study was to use real-time pressure recording and high temporal resolution two-dimensional oxygen imaging to investigate the hydraulic activity of *A. marina*, with regard to directionality and frequency. Directionality in this case affects sediment porewater pressurization (Wethey et al. 2008), with implications for porewater bioadvection and redox oscillation at depth as well as in surficial sediments (Figs. 6, 7).

Hydraulic activities of the lugworm induced behavior-specific pressure fluctuations around the hydrostatic baseline, which drive oscillatory porewater bioadvection. An increase in the porewater pressure accompanies oxygenation of the sediment surrounding the burrow and an emergence of suboxic or anoxic porewater through the sediment surface (Fig. 2). Inversely, pressure reduction causes porewater movement toward the lugworm and the oxygenation of the surficial sediments as a result of the inflow of overlying oxic water (Figs. 2, 4). Hydraulic behaviors by arenicolid polychaetes, comprising positive and negative porewater pressure waveforms, have been documented for unrestrained individuals in the field as well as in aquaria in the laboratory (Wethey et al. 2008; Woodin and Wethey 2009). Additionally, we have recorded comparable pressure and oxygen oscillations in the presence of several abundant and geographically widespread types of macrobenthic species, e.g., tellinid bivalves and thalassinid crustaceans (authors with T. DeWitt unpubl. data). The oscillatory character of geochemical conditions induced by porewater bioadvection may thus be a predominant feature of biogenic active sediments.

The activities of macrofauna clearly affect sediments, directly by inducing porewater advection and indirectly by increasing the area over which diffusive transport occurs (Waldbusser and Marinelli 2006). In permeable sediments, biohydraulic activities of macrofauna move water within the burrow lumen as well as induce porewater advection in the sediment surrounding the burrow. Porewater bioadvection leads to enhanced exchange of solutes between sediment and the overlying water and affects larger sediment volumes than those affected by diffusion (Meysman et al. 2005; Timmerman et al. 2006; Wethey et al. 2008). Thus, in this sense, porewater bioadvection is similar to purely physical forces that induce intensive sediment percolation, including wave action or advection driven by physical topography or biogenic topography (Huettel et al. 1996; Precht et al. 2004). But there are also important differences. Physical forces are typically restricted to the upper 5 cm, while the zone of influence of the bioadvective forces can be much greater, driving oxygenation of the upper few centimeters of the sediment as well as of the sediment volumes 10–20 cm below the surface (Fig. 3; Meysman et al. 2007; Wethey et al. 2008). A critical difference is that bioadvective forces depend upon the activities of an organism. Given temporal persistence of burrow structures and animal activities for days to weeks, as is true, e.g., of the arenicolid *Abarenicola pacifica* (Krager and Woodin 1993), and considering hydraulic activities that reverse or stop on the scale of minutes (Wethey et al. 2008; Woodin and Wethey 2009), the zone influenced by an arenicolid individual will experience redox oscillations on the scale of minutes potentially for days. Some areas will be more affected than others (Fig. 6), and the scale of the effects will strongly depend on the hydraulic conductivity of the

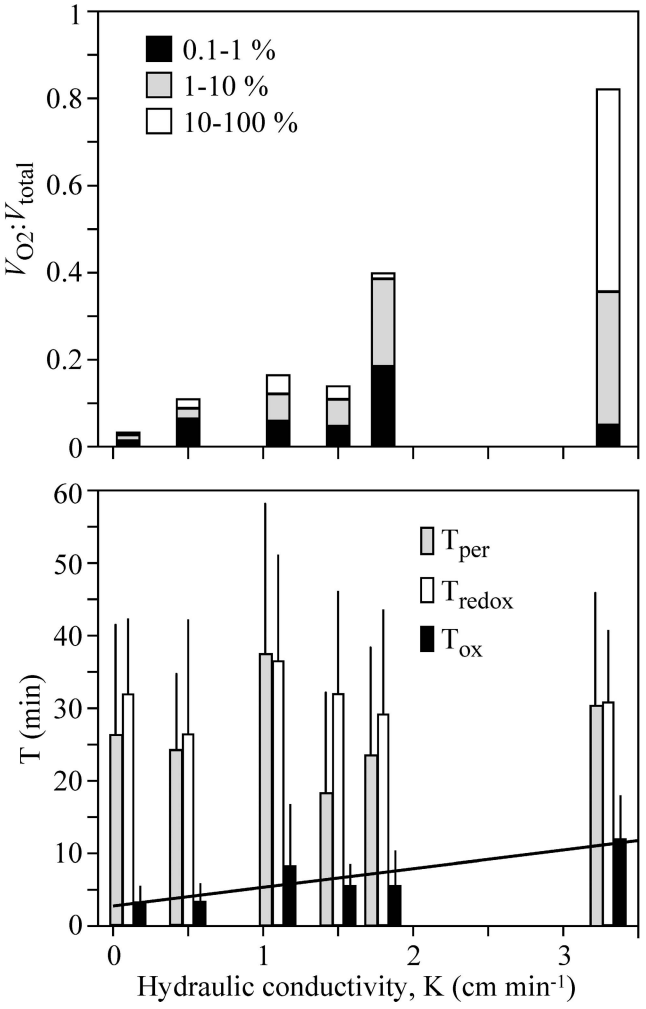

Fig. 7. (A) Sediment volume that was oxygenated during the 48-h measurement with probability of at least 0.1% (i.e., for at least ~ 3 min; $V_{O_2} = V_{O_2deep}$ and $V_{O_2surface}$), expressed relative to the total sediment volume in the aquarium (V_{total}). The oxygenated sediment volumes were differentiated according to the oxygenation probabilities (e.g., gray bars correspond to the proportion of sediment oxygenated with probabilities between 1% and 10%) and were calculated from images in Fig. 6. (B) Means and standard deviations relative to the hydraulic conductivity of the following: (1) the time intervals between bouts of sediment pressurization due to lugworm pumping activity (T_{per}), (2) the time intervals in which individual pixels experienced oxic conditions (T_{ox}, $O_2 \geq 5\%$ air saturation), and (3) the temporal period of redox oscillation for each pixel ($T_{redox} = T_{anox} + T_{ox}$; T_{anox}, $O_2 < 5\%$ AS). The means and standard deviations of T_{ox} and T_{redox} were calculated only for pixels with detectable redox oscillations, as derived from the oxygen dynamics in the sediment detected by the planar optode and confirmed by the directionality predictions based on the pressure records. The regression line is for T_{ox} vs. sediment permeability (linear regression, $r^2 = 0.918$, $p \leq 0.01$).

sediment (Fig. 7; Table 2). Unlike physical advection, which is typically linked to water movements driven by wind, tides, and other large-scale forces, porewater bioadvection depends on the local phenomenon of the presence of the generating organism, its density, and its state of activity. We expect that in permeable sediments in the field, physical and biological advection are additive, i.e., the spatially and temporally highly variable bioadvection may be superposed on a smoother and slower physical, wave and/or topography driven percolation.

Our results show that some qualitative phenomena linked to biohydraulic activities, as well as the relative importance of biogenic diffusive vs. advective transport of solutes such as oxygen, strongly depend on sediment permeability. In highly permeable sandy sediment, porewater bioadvection induced massive oxygenation of sediment at depth, with ~ 50% of the sediment volume in the aquarium experiencing oxygen for at least 10% of the time during the 48-h measurement (Fig. 6). In this study, we only tested a single specimen in this highly permeable sediment, but we have also detected comparable massive and persistent oxygenation at depth in larger tanks with multiple lugworms present in similarly permeable sediments (N. Volkenborn unpubl. data). The probability and extent of sediment oxygenation were considerably lower in less permeable sediments with higher oxygen consumption rates (Figs. 2, 6; Table 1).

The comparison of oxygen budgets in different sediment types indicates that the excess oxygen, i.e., oxygen not used for lugworm respiration, is predominantly consumed in the advective zone surrounding the gallery and the feeding pocket in highly permeable sediments, while diffusive uptake through the burrow wall is the dominant O_2 transport mechanism from the burrow into the surrounding sediment at low permeabilities (Table 2). Our results from intermediate permeability sediments are consistent with those of Timmermann et al. (2006), who also found that lugworms use roughly 49% of the pumped oxygen for their respiration, while 23% and 28% of the pumped oxygen are consumed by diffusive uptake through the burrow wall and in the advective zone, respectively. Surprisingly, pumping rates estimated from the oxygen budget as well as based on the changing volume of the oxygenated sediment at depth were highest for the most permeable sediment (Table 2). This result should be interpreted with caution because of the possible overestimation of the OCR of a frequently oxygenated sediment (Polerecky et al. 2005), indicating the limitations of using the planar optode technology to derive pumping rates from oxygen imaging. However, in this context it should also be noted that in very permeable sediments the pumped water easily moves away from the animal and thus the oxygen cannot be efficiently used for respiration. On the other hand, owing to the lower resistance to flow, the power required to pump water into highly permeable sediment is considerably smaller (Meysman et al. 2005). This inverse relationship between the oxygen use efficiency and "workout" necessary to pump the oxygen-rich water may explain why lugworms are able to inhabit a large variety of sediment types, but further experiments on the bioenergetics of hydraulic activity in different sediments types are necessary to better understand this aspect.

Pressurization of the most permeable sediment led to approximately even sediment percolation, with porewater exiting at the sediment–water interface as a sheet of flow raising the oxic–anoxic boundary above the sediment–water interface (Fig. 3). In contrast, in low-permeability

sediments, porewater emerged at the sediment–water interface as ''jetlike'' anoxic plumes, locally raising the oxic–anoxic boundary (Figs. 2, 3). It is likely that this enhanced and localized porewater transport occurred through cracks, i.e., sediment volumes with locally increased permeability. Boudreau et al. (2005) and Dorgan et al. (2008) described the formation of cracks in gels such as muds when force is applied without the injection of water. In sediments with larger grain size than muds we have seen similar cracks in the presence of other arenicolids and tellinid bivalves (authors' unpubl. data). We think that the crack formation by pressurization of the sediment through water injection is a characteristic feature of medium- to low-permeability sediments. Interestingly, the infiltration of overlying water into the surficial sediment appeared to occur rather homogenously during backward pumping, while suboxic and anoxic water exited the sediment as plumes localized through cracks during pressurization (Web appendix, Video 4). This asymmetry indicates that cracks are not stagnant channels but open, closed, and reopened by bidirectional porewater bioadvection.

It is possible that the emergence of the jetlike anoxic plumes above the sediment surface was induced or facilitated by the activity of meiofauna. The sediment in our experiments was not defaunated and probably contained diverse meiofaunal organisms, which can have significant effects on interstitial solute transport (Aller and Aller 1992; Glud and Fenchel 1999). Also, burrows made by small organisms may serve as channels through which increased porewater flow can occur, thereby acting as sedimentary cracks. However, we did not observe any obvious signs of meiofaunal activities at the transparent plate of our aquaria, and we never detected similar oxygen dynamics in the same sediment without the lugworm present, nor did we detect any sediment pressurization phenomena. It is therefore unlikely that the principal contrasting character of porewater flow in the different sediments was associated with meiofauna.

In addition to sediment pressurization, which typically occurs as the lugworm pumps water into the sediment through the tail shaft and pushes it into the open pore space surrounding the feeding pocket, we frequently observed intensive and durable sediment underpressurization that led to porewater flows in a reverse direction (Fig. 4). Based on the measured sedimentary oxygen consumption rates, purely diffusive oxygen penetration would be limited to the upper 0.4 and 0.9 mm in the low- and high-permeability sediments, respectively (Table 1). However, during underpressurization, oxygen penetrated significantly deeper over most of the sediment surface with a maximum penetration of 0.28 and 2.55 cm in the low- and high-permeability sediments (Fig. 4; Table 1). Similar variability in oxygen penetration was observed by in situ oxygen microsensor measurements conducted in a lugworm populated site even several centimeters away from the lugworm burrows, in contrast to a rather constant oxygen penetration in the sediment without the lugworm (Volkenborn et al. 2007). Such variance is to be expected if lugworm behavior is temporally variable both in magnitude and direction, as is seen in field recordings (Wethey et al. 2008).

Prima facie, the phenomenon of reversed pumping seemed peculiar, exposing the lugworm to anoxic porewater from the surrounding sediment, which was then moved out of the sediment via the tail shaft. However, this behavior may serve as a mechanism to loosen packed particles and redistribute fine particles that may have clogged the lugworm's connection to the surface during periods of forward pumping. This would be similar to the strategy of engineers in cleaning filters by reverse-flow wash in upward flow sand filtration (Baker and Taras 1981).

The emergence of anoxic and potentially nutrient-rich porewater from below during sediment pressurization, either in a sheetlike or jetlike manner, may have substantial implications for sediment biology. It can serve, e.g., as a chemical cue during benthic recruitment (Marinelli and Woodin 2002), as a fertilizer of localized microalgal growth (Marinelli 1992), or as a signal allowing prey localization (Weissburg et al. 2002). For example, for recruiting polychaetes it was found that the decision to burrow at a given locale is made within 30 s after the first contact with the sediment surface (Woodin et al. 1995), and the decision is strongly affected by the geochemical signals (Woodin et al. 1998). Many of these ecological processes take place on timescales of seconds to minutes and may therefore well be affected by temporal geochemical dynamics at the sediment–water interface that are induced by the hydraulic activities of organisms at depth.

With respect to temporal patterns in the pumping activity, our results confirm the findings of previous studies on the lugworm *A. marina*, which have detected irrigation patterns with a typical periodicity of 30 min (Wells 1953; Krüger 1964; Timmermann et al. 2006). However, our results suggest that this activity pattern does not consist of periods of active irrigation followed by intervals where the activity, and thus the porewater bioadvection, would completely cease. We did not find long resting periods in our pressure recordings. Instead, periods of pressurization were typically followed by periods of underpressurization, which were associated with defecation events, burrowing episodes, or backward pumping (Figs. 2, 4). This has implications for experiments that use inert tracers to estimate pumping rates of lugworm irrigation (Timmermann et al. 2003; Meysman et al. 2007; Na et al. 2008). Although giving a good first approximation for volumes pumped, such time-integrated approaches conceal backward flow and thus may lead to an underestimation of pumping rates. Furthermore, porewater pressure transients on the scale of seconds, such as individual large pressure pulses (Fig. 2, burrowing and defecation), and on the scale of minutes, such as the switching between pressurization and underpressurization of the sediment (Fig. 4), have important implications for the geochemical variations and impose physical forces that influence sediment integrity. Time-averaged pumping rates and the assumption of continuous unidirectional flow do not account for these effects, and, given their implications for rates of reaction, we suggest that metrics used to characterize biogenic hydraulic activities need to explicitly include the oscillatory character of hydraulic porewater bioadvection.

Our measurements demonstrate that, owing to flow reversals and variable hydraulic activity, sediments experi-

ence highly dynamic redox oscillations (Figs. 6, 7). We typically detected oxygen concentration of $< 20\%$ air saturation at the aquarium wall millimeters to centimeters away from the burrow. These are reasonable concentrations, considering that the tail shaft of the lugworm burrow is typically filled with water with an oxygen concentration of $> 80\%$ air saturation during irrigation, and approximately 40–60% of this oxygen is respired by the worm in all but the most permeable sediments (Table 2; Timmermann et al. 2006). There are a number of models that provide us with a good understanding of the effects of bioirrigation on the biogeochemical processes in the sediments (Meysman et al. 2006*b*), especially when considering long timescales. However, since these models assume that bioirrigation is unidirectional and has a constant rate, they do not account for the possibility of redox oscillations on short timescales, and thus exclude mechanisms that may play an important biogeochemical role. Discontinuous irrigation results in highly variable oxygen distribution (Timmermann et al. 2006), and the resultant redox oscillations are known to be important drivers of remineralization (Aller 1994; Sun et al. 2002). Such perturbations in microenvironmental conditions may also result in the release of intermediates in vital metabolic pathways (e.g., NO and/or N_2O during denitrification; Schreiber et al. 2009; Stief et al. 2009). Our study shows that redox oscillations in sediments inhabited by the lugworm *A. marina* typically occur on the timescale of minutes and may affect substantial sediment volumes that increase approximately linearly with sediment permeability (Fig. 7). This temporal scale of redox oscillations may significantly affect the microbial diversity and activity in the sediment and thus have potentially large environmental implications. We suggest that improved bioirrigation models need to include this conceptual mechanism to more adequately describe the effects of bioirrigation on sediment biogeochemistry.

Methodological limitations—In this study, we used sandwich aquaria to monitor effects of the lugworm activity on biogeochemical processes in different sediment types. On the one hand, this experimental approach enabled us to synchronously obtain complementary information about animal behavior, porewater pressure variations, and oxygen distributions. On the other hand, this configuration potentially affected the animal or may have introduced artifacts in the solute dynamics within the sediment as a result of the geometrical constraints imposed on the porewater transport. We used a number of approximations to apply this information in a quantitative manner and extract meaningful parameters that could potentially be applied also under unconstrained, natural settings. Here we indicate when caution needs to be exercised with data interpretation.

Owing to the geometric constraints, the magnitude and spatial extent of the new phenomena identified in this study (e.g., the emergence of sheetlike flow or jetlike plumes of anoxic water at the sediment surface during forward pumping, enhanced and highly dynamic oxygenation of deep and surficial sediment during forward and backward pumping, respectively) need to be viewed with caution. However, our conclusion that these phenomena do occur and are important in a variety of sediment types remains valid. Many of these phenomena were independently observed by different methods (planar oxygen optodes, pressure sensors, and visual imagery) and matched to visible and repeatable behaviors by the worms. This is clear from Figs. 2, 4 where the time synchronous optode and pressure sensor signals are complementary to the indicated behaviors. Both the direction and temporal durations of activities could be confirmed independently by at least two methods in all cases. Wethey et al. (2008) had previously shown that the temporal variations of the pressure transients do not depend on the geometry employed. Extrapolation of the calculated rates and consumptions to the unconstrained case may be problematic in some cases; however, the patterns of bioadvective porewater transients are real and consistent with observations in the field (Wethey et al. 2008).

Clearly, the shape of the oxygenated sediment volumes, V_{O_2deep}, and the porewater flow fields were strongly deformed because of the close proximity of the aquarium walls. However, because the inhibition of porewater flow in the direction perpendicular to the wall needs to be compensated by an increased flow along the wall, we expect that our approximation of V_{O_2deep} by a sphere without caps (Fig. 1A) leads to values comparable to the unconstrained situation, especially in sediments with high and intermediate permeabilities. The discrepancy between our estimates and a situation in unconstrained sediments may be larger for the low-permeability and high-OCR sediments, where oxygen is less likely to reach the optode, and oxygenated spheres with volumes below ~ 0.9 cm^3 are not detected by the sensor if water injection occurs in the center of the aquarium (*see* probability plots in Fig. 6). Consequently, average values for V_{O_2deep} in these sediments probably underestimate the oxygenated volume at depth. However, because measurements lasted for ~ 2 d, during which the lugworm had presumably numerous opportunities to move and pump both closer to (leading to overestimated V_{O_2deep}) and farther away from the optode (leading to underestimated V_{O_2deep}), we believe that our results reflect at least the correct range of time-averaged values of V_{O_2deep} also for these sediment types. This assumption is consistent with our models of unconstrained, behaviorally realistic, bioadvective porewater flows in the field, which estimated that large subsurface regions would be flushed each day (Wethey et al. 2008), and the shapes of these flushed regions were similar to those observed in the optode imagery.

It is known that the biotic and abiotic contributions to the sedimentary OCR can vary during multiple flushings of the same sediment volume (Polerecky et al. 2005). This is because reduced compounds that had accumulated in the sediment during anoxic conditions (e.g., iron sulfides) contribute substantially to the total sedimentary oxygen consumption, and once the amount or reactivity of these compounds decreases as a result of their oxidation, the total OCR will also decrease. We tested this scenario in our aquaria and found that OCR values calculated for sediment volumes oxygenated by the lugworm activity, estimated

from images recorded during the long-term incubations, were up to 12-fold lower than those obtained from the manual injection measurements conducted in a previously nonoxygenated sediment volume in the same aquarium. It should be noted, however, that this discrepancy is probably exaggerated because the former values were obtained from images measured during intervals when the lugworm activity did not completely cease (implied by the simultaneous pressure recordings), which led to likely underestimated OCR values. Furthermore, the two-dimensional OCR maps derived from the manual injection measurements exhibited large spatial heterogeneity, with OCR values varying by several tens of percent on the scales of millimeters (data not shown). These examples show that the OCR values determined around bioirrigated burrows and the quantities derived from them (e.g., instantaneous pumping rates, oxygen budgets) must be considered as approximations and thus be interpreted with caution.

Estimates of time-integrated and instantaneous pumping rates derived from the oxygen budget calculations and the wax and wane of V_{O_2deep}, respectively, are in the realistic range and consistent with those reported by other investigators (Riisgård and Banta 1998; Kristensen 2001; Timmermann et al. 2006). However, owing to the methodological limitations described above (e.g., spatial constraints, variable OCR), estimates of pumping rates solely based on planar optode imaging of oxygen need to be interpreted with caution. As discussed by Polerecky et al. (2006), oxygen extends farther and lasts longer at the wall than would be the case if the wall was absent, resulting in an overestimation of V_{O_2deep}. Contrary, the volumes will be underestimated at larger distances between burrow and sensor, especially if high sedimentary OCR or low sediment permeability prevents oxygen from reaching the planar optode. These are generally acknowledged drawbacks of the planar optode technique (Polerecky et al. 2006; Glud 2008). Considering that the aquarium width (1.2 cm) was only slightly larger than the measured range of lugworm diameters (1.0–1.2 cm) and that the transport of oxygen by bioadvection dramatically exceeded its consumption in the high-permeability and low-OCR sediments, we expect that our estimates of V_{O_2deep} in these sediments are fairly accurate. This is suggested also by the fact that the pumping rates derived from the dynamics of V_{O_2deep} were comparable to those reported in the literature at similar conditions. In concert with traditional techniques of pump rate measurements (e.g., tracer experiments, Meysman et al. 2007; worms in glass tubes, Riisgård and Banta 1998; thermistor probes, Timmermann et al. 2006; or porewater pressure sensors, Wethey and Woodin 2005) the planar optode technology yields vital information about the spatiotemporal dynamics of porewater flow and solute dynamics.

In conclusion, this study presents evidence for qualitatively new phenomena associated with the biohydraulic activity of the lugworm *A. marina*, specifically (1) frequent periods of biogenic reduction in porewater pressure below hydrostatic baseline, resulting in reverse porewater flow (Fig. 4); (2) the striking difference between the sheetlike and jetlike patterns in the outflow of the overlying water from high-permeability and low-permeability sediments, respectively, associated with biogenic pressurization of the sediments (Fig. 3); and (3) the realization that the O_2 distributions around bioirrigated burrows are dynamically changing in a very broad range, both temporally (between minutes and hours) and spatially (between a few millimeters and several centimeters) (Figs. 6, 7). Lasting pressurization of the sediment, transient bursts of activity, biohydraulic sediment cracking, forward and reversed advective pulses, and long-term flow reversals all contribute to very dynamic geochemical conditions in biogenically active sediments. We focused on lugworms, but the underlying mechanisms and the associated phenomena also apply to many other benthic organisms living in sandy mud, muddy sand, and sandy sediments. Furthermore, we focused on the dynamics of oxygen, primarily because it is the most important electron acceptor for benthic mineralization and is essential for the respiratory processes for benthic organisms; however, it is likely that infaunal hydraulic activities induce similar dynamics in the distribution of other porewater solutes (e.g., nitrate, sulphate, sulphide). The spatial extent of bioadvectional transport and the temporal dynamics will differ among chemical species with varying reactivity. Porewater bioadvection may thus play an important role in sediment biogeochemistry, microbial diversity, and benthic ecology. Hopefully this study will act as a stimulus for more investigations into the dynamics of porewater bioadvection in aquatic sediments and its implications for the functioning of benthic ecosystems.

Acknowledgments

We thank Karsten Reise and Dirk de Beer for support during this collaborative study; Jerry Hilbish, George Matsui, Filip Meysman, Ronnie Glud, and one anonymous reviewer made valuable comments on the manuscript; Elisabeth Herre provided logistical support; Arthur Illingworth and Allen Frye designed and built the aquaria. The provision of infrastructure and lab space by the Alfred Wegener Institute for Polar and Marine Research and by the Max-Planck-Institute for Marine Microbiology is greatly appreciated. Financial support was provided by the German Ministry for Education and Research, the Max-Planck Society, and grants from the U.S. Office of Naval Research (N00014-0310352), the U.S. National Aeronautics and Space Administration (NNG04GE43G), the U.S. National Oceanic and Atmospheric Administration (NA 04 NOS 4780264), and the U.S. National Science Foundation OCE 0928002.

References

Aller, R. C. 1980. Quantifying solute distributions in the bioturbated zone of marine sediments by defining an average micro-environment. Geochim. Cosmochim. Acta **44:** 1955–1965, doi:10.1016/0016-7037(80)90195-7

———. 1983. The importance of the diffusive permeability of animal burrow linings in determining marine sediment chemistry. J. Mar. Res. **41:** 299–322, doi:10.1357/002224083788520225

———. 1994. Bioturbation and remineralization of sedimentary organic matter: Effects of redox oscillation. Chem. Geol. **114:** 331–345, doi:10.1016/0009-2541(94)90062-0

———. 2001. Transport and reactions in the bioirrigated zone, p. 269–301. *In* B. P. Boudreau and B. B. Jørgensen [eds.], The benthic boundary layer: Transport processes and biogeochemistry. Oxford Univ. Press.

———, AND J. Y. ALLER. 1992. Meiofauna and solute transport in marine muds. Limnol. Oceanogr. **37:** 1018–1033.

———, AND J. Y. YINGST. 1978. Biogeochemistry of tube-dwellings: A study of the sedentary polychaete *Amphitrite ornata* (Leidy). J. Mar. Res. **36:** 201–254.

BAKER, M. N., AND M. J. TARAS. 1981. The quest for pure water: A history of the twentieth Century, volume 1. American Water Works Association.

BOUDREAU, B. P. 1996. The diffusive tortuosity of fine-grained unlithified sediments. Geochim. Cosmochim. Acta **60:** 3139–3142, doi:10.1016/0016-7037(96)00158-5

———. 1998. Mean mixed depth of sediments: The wherefore and the why. Limnol. Oceanogr. **43:** 524–526.

———, AND OTHERS. 2005. Bubble growth and rise in sediments. Geology **33:** 517–520.

CADÉE, G. C. 2001. Sediment dynamics by bioturbating organisms, p. 127–148. *In* K. Reise [ed.], Ecological comparisons of sedimentary shores. Ecological Studies, vol. 151. Springer.

CANFIELD, D. E., AND OTHERS. 1993. Pathways of organic carbon oxidation in three continental margin sediments. Mar. Geol. **113:** 27–40, doi:10.1016/0025-3227(93)90147-N

DORGAN, K. M., S. R. ARWADE, AND P. A. JUMARS. 2008. Worms as wedges: Effects of sediment mechanics on burrowing behavior. J. Mar. Res. **66:** 219–254, doi:10.1357/002224008785837130

GLUD, R. N. 2008. Oxygen dynamics in marine sediments. Mar. Biol. Res. **4:** 243–289, doi:10.1080/17451000801888726

———, AND T. FENCHEL. 1999. The importance of ciliates for interstitial solute transport in benthic communities. Mar. Ecol. Prog. Ser. **186:** 87–93, doi:10.3354/meps186087

———, N. B. RAMSING, J. K. GUNDERSEN, AND I. KLIMANT. 1996. Planar optodes: A new tool for fine scale measurements of two dimensional O_2 distribution in benthic communities. Mar. Ecol. Prog. Ser. **140:** 217–226, doi:10.3354/meps140217

HOLST, G., AND B. GRUNWALD. 2001. Luminescence lifetime imaging with transparent oxygen optodes. Sens. Actuators B **74:** 78–90, doi:10.1016/S0925-4005(00)00715-2

HUETTEL, M., W. ZIEBIS, AND S. FORSTER. 1996. Flow-induced uptake of particulate matter in permeable sediments. Limnol. Oceanogr. **41:** 309–322.

JØRGENSEN, B. B., AND N. P. REVSBECH. 1985. Diffusive boundary layers and the oxygen uptake of sediments and detritus. Limnol. Oceanogr. **30:** 111–122.

JUMARS, P. A., AND R. A. WHEATCROFT. 1989. Responses of benthos to changing food quality and quantity, with a focus on deposit feeding and bioturbation, p. 235–253. *In* W. Berger and G. Wefer [eds.], Productivity of the ocean: Present and past. John Wiley.

KLUTE, A., AND C. DIRKSEN. 1986. Hydraulic conductivity and diffusivity: Laboratory methods, p. 687–700. *In* A. Klute [ed.], Methods of soil analysis, part 1, physical and mineralogical methods. American Society of Agronomy.

KOGURE, K., AND M. WADA. 2005. Impacts of macrobenthic bioturbation in marine sediment on bacterial metabolic activity. Microbes Environ. **20:** 191–199, doi:10.1264/jsme2.20.191

KRAGER, C. D., AND S. A. WOODIN. 1993. Spatial persistence and sediment disturbance of an arenicolid polychaete. Limnol. Oceanogr. **38:** 509–520.

KRISTENSEN, E. 1988. Benthic fauna and biogeochemical processes in marine sediments: Microbial activities and fluxes, p. 275–299. *In* T. H. Blackburn and J. Sørensen [eds.], Nitrogen cycling in coastal marine environments. John Wiley.

———. 2001. Impact of polychaetes (*Nereis* spp. and *Arenicola marina*) on carbon biogeochemistry in coastal marine sediments. Geochem. Trans. **2:** 92–103, doi:10.1186/1467-4866-2-92

KRÜGER, F. 1964. Experiments concerning the dependence of respiration of *Arenicola marina* (Annelides Polychaeta) on size and temperature. Helgol. Wiss. Meeresunters **10:** 38–63. [In German.], doi:10.1007/BF01626097

KÜHL, M., AND L. POLERECKY. 2008. Functional and structural imaging of phototrophic microbial communities and symbioses. Aquat. Microb. Ecol. **53:** 99–118, doi:10.3354/ame01224

LOHRER, A. M., S. F. THRUSH, AND M. M. GIBBS. 2004. Bioturbators enhance ecosystem function through complex biogeochemical interactions. Nature **431:** 1092–1095, doi:10.1038/nature03042

MARINELLI, R. L. 1992. Effects of polychaetes on silicate dynamics and fluxes in sediments: Importance of species, animal activity and polychaete effects on benthic diatoms. J. Mar. Res. **50:** 745–779, doi:10.1357/002224092784797566

———, AND S. A. WOODIN. 2002. Experimental evidence for linkages between infaunal recruitment, disturbance, and sediment surface chemistry. Limnol. Oceanogr. **47:** 221–229.

MEYSMAN, F. J. R., O. S. GALAKTIONOV, P. L. M. COOK, F. JANSSEN, M. HUETTEL, AND J. J. MIDDELBURG. 2007. Quantifying biologically and physically induced flow and tracer dynamics in permeable sediments. Biogeosciences **4:** 627–646.

———, ———, B. GRIBSHOLT, AND J. J. MIDDELBURG. 2006b. Bioirrigation in permeable sediments: An assessment of model complexity. J. Mar. Res. **64:** 589–627, doi:10.1357/002224006778715757

———, ———, AND J. J. MIDDELBURG. 2005. Irrigation patterns induced in permeable sediments by burrow ventilation: A case study of *Arenicola marina*. Mar. Ecol. Prog. Ser. **303:** 195–212, doi:10.3354/meps303195

———, J. J. MIDDELBURG, AND C. H. R. HEIP. 2006a. Bioturbation: A fresh look at Darwin's last idea. Trends Ecol. Evol. **21:** 688–695, doi:10.1016/j.tree.2006.08.002

NA, T., B. GRIBSHOLT, O. S. GALAKTIONOV, T. LEE, AND F. J. R. MEYSMAN. 2008. Influence of advective bio-irrigation on carbon and nitrogen cycling in sandy sediments. J. Mar. Res. **66:** 691–722, doi:10.1357/002224008787536826

PEARSON, T. H. 2001. Functional group ecology in soft-sediment marine benthos: The role of bioturbation. Oceanogr. Mar. Biol. Annu. Rev. **39:** 233–267.

POLERECKY, L., U. FRANKE, U. WERNER, B. GRUNWALD, AND D. DE BEER. 2005. High spatial resolution measurement of oxygen consumption rates in permeable sediments. Limnol. Oceanogr.: Methods **3:** 75–85.

———, N. VOLKENBORN, AND P. STIEF. 2006. High temporal resolution oxygen imaging in bioirrigated sediments. Environ. Sci. Technol. **40:** 5763–5769, doi:10.1021/es0604941

PRECHT, E., U. FRANKE, L. POLERECKY, AND M. HUETTEL. 2004. Oxygen dynamics in permeable sediments with wave-driven pore water exchange. Limnol. Oceanogr. **49:** 693–705.

REISE, K. 1983. Biotic enrichment of intertidal sediments by experimental aggregates of the deposit-feeding bivalve *Macoma balthica*. Mar. Ecol. Prog. Ser. **12:** 229–236, doi:10.3354/meps012229

RIISGÅRD, H. U., AND G. T. BANTA. 1998. Irrigation and deposit feeding by the lugworm *Arenicola marina*, characteristics and secondary effects on the environment. A review of our current knowledge. Vie Milleu **48:** 243–257.

———, AND P. S. LARSEN. 2005. Water pumping and analysis of flow in burrowing zoobenthos: An overview. Aquat. Ecol. **39:** 237–258, doi:10.1007/s10452-004-1916-x

ROSENBERG, R. 2001. Marine benthic faunal successional stages and related sedimentary activity. Sci. Mar. **65:** 107–119, doi:10.3989/scimar.2001.65s2107

Schreiber, F., B. Loeffler, L. Polerecky, M. M. Kuypers, and D. de Beer. 2009. Mechanisms of transient nitric oxide and nitrous oxide production in a complex biofilm. The ISME Journal **3:** 1301–1313, doi:10.1038/ismej.2009.55

Snelgrove, P. V. R., and others. 1997. The importance of marine sediment biodiversity in ecosystem processes. Ambio **26:** 578–583.

Stief, P., M. Poulsen, L. P. Nielsen, H. Brix, and A. Schramm. 2009. Nitrous oxide emission by aquatic macrofauna. Proc. Natl. Acad. Sci. U.S.A. **106:** 4296–4300, doi:10.1073/pnas.0808228106

Sun, M. Y., R. C. Aller, C. Lee, and S. G. Wakeham. 2002. Effects of oxygen and redox oscillation on degradation of cell-associated lipids in surficial marine sediments. Geochim. Cosmochim. Acta **66:** 2003–2012, doi:10.1016/S0016-7037(02)00830-X

Teal, L. R., M. T. Bulling, E. R. Parker, and M. Solan. 2008. Global patterns of bioturbation intensity and mixed depth of marine soft sediments. Aquat. Biol. **2:** 207–218.

Thamdrup, B., and D. E. Canfield. 2000. Benthic respiration in aquatic systems, p. 86–103. *In* O. E. R. Sala, R. B. Jackson, H. A. Mooney and R. W. Horwarth [eds.], Methods in ecosystem science. Springer.

Thayer, C. W. 1979. Biological bulldozers and the evolution of marine benthic communities. Science **203:** 458–461, doi:10.1126/science.203.4379.458

Timmermann, K., G. T. Banta, and R. N. Glud. 2006. Linking *Arenicola marina* irrigation behavior to oxygen transport and dynamics in sandy sediments. J. Mar. Res. **64:** 915–938, doi:10.1357/002224006779698378

———, ———, J. Larsen, and O. Andersen. 2003. Modelling particle and solute transport in sediments inhabited by *Arenicola marina*. Effects of pyrene on transport processes. Vie et Milieu **53:** 187–200.

———, J. Christensen, and G. T. Banta. 2002. Modeling of advective solute transport in sandy sediments inhabited by the lugworm *Arenicola marina*. J. Mar. Res. **60:** 151–169, doi:10.1357/002224002762341285

Volkenborn, N., L. Polerecky, S. I. C. Hedtkamp, J. E. E. van Beusekom, and D. de Beer. 2007. Bioturbation and bioirrigation extend the open exchange regions in permeable sediments. Limnol. Oceanogr. **52:** 1898–1909.

Waldbusser, G. G., and R. L. Marinelli. 2006. Macrofaunal modification of porewater advection: The role of species function, species interaction, and kinetics. Mar. Ecol. Prog. Ser. **311:** 217–231, doi:10.3354/meps311217

Weissburg, M. J., M. C. Ferner, D. P. Pisut, and D. L. Smee. 2002. Ecological consequences of chemically mediated prey perception. J. Chem. Ecol. **28:** 1953–1970, doi:10.1023/A:1020741710060

Wells, G. P. 1953. Defecation in relation to the spontaneous activity cycles of *Arenicola marina* L. J. Mar. Biol. Assoc. U.K. **32:** 51–63, doi:10.1017/S0025315400011425

———. 1963. Barriers and speciation in lugworms (Arenicolidae, Polychaeta), p. 79–98. *In* J. P. Harding and N. Tebble [eds.], Speciation in the Sea, No. 5. The Systematics Association.

Wethey, D. S., and S. A. Woodin. 2005. Infaunal hydraulics generate pore-water pressure signals. Biol. Bull. **209:** 139–145, doi:10.2307/3593131

———, ———, N. Volkenborn, and K. Reise. 2008. Pore-water advection by hydraulic activities of lugworms, *Arenicola marina*: A field, laboratory and modeling study. J. Mar. Res. **66:** 255–273, doi:10.1357/002224008785837121

Wittmann, A. C., M. Schröer, C. Bock, H.-U. Steeger, R. J. Paul, and H.-O. Pörtner. 2008. Indicators of oxygen and capacity limited thermal tolerance in the lugworm *Arenicola marina*. Clim. Res. **37:** 227–240.

Woodin, S. A., S. M. Lindsay, and D. S. Wethey. 1995. Process-specific recruitment cues in marine sedimentary systems. Biol. Bull. **189:** 49–58, doi:10.2307/1542201

———, R. L. Marinelli, and S. M. Lindsay. 1998. Process-specific cues for recruitment in sedimentary environments: Geochemical signals? J. Mar. Res. **56:** 535–558, doi:10.1357/002224098321822410

———, and D. S. Wethey. 2009. Arenicolid behaviors: Similarity of *Arenicola marina* and *Abarenicola pacifica*. Zoosymposia **2:** 447–456.

Ziebis, W., S. Forster, M. Huettel, and B. B. Jørgensen. 1996. Complex burrows of the mud shrimp *Callianassa truncata* and their geochemical impact in the sea bed. Nature **382:** 619–622, doi:10.1038/382619a0

Associate editor: Ronnie Nøhr Glud

Received: 01 October 2009
Accepted: 24 December 2009
Amended: 25 January 2010